Signature of altered retinal microstructures and electrophysiology in schizophrenia spectrum disorders is associated with disease severity and polygenic risk

Emanuel Boudriot, Vanessa Gabriel, David Popovic, Pauline Pingen, Vladislav Yakimov, Sergi Papiol, Lukas Roell, Genc Hasanaj, Simiao Xu, Joanna Moussiopoulou, Siegfried Priglinger, Christoph Kern, Eva C. Schulte, Alkomiet Hasan, Oliver Pogarell, Peter Falkai, Andrea Schmitt, Benedikt Schworm, Elias Wagner

Angaben zur Veröffentlichung / Publication details:

Boudriot, Emanuel, Vanessa Gabriel, David Popovic, Pauline Pingen, Vladislav Yakimov, Sergi Papiol, Lukas Roell, et al. 2024. "Signature of altered retinal microstructures and electrophysiology in schizophrenia spectrum disorders is associated with disease severity and polygenic risk." Biological Psychiatry 96 (10): 792–803. https://doi.org/10.1016/j.biopsych.2024.04.014.

Biological Psychiatry

Archival Report

Signature of Altered Retinal Microstructures and Electrophysiology in Schizophrenia Spectrum Disorders Is Associated With Disease Severity and Polygenic Risk

Emanuel Boudriot, Vanessa Gabriel, David Popovic, Pauline Pingen, Vladislav Yakimov, Sergi Papiol, Lukas Roell, Genc Hasanaj, Simiao Xu, Joanna Moussiopoulou, Siegfried Priglinger, Christoph Kern, Eva C. Schulte, Alkomiet Hasan, Oliver Pogarell, Peter Falkai, Andrea Schmitt, Benedikt Schworm, CDP Working Group, Elias Wagner, Daniel Keeser, and Florian J. Raabe

ABSTRACT

BACKGROUND: Optical coherence tomography and electroretinography studies have revealed structural and functional retinal alterations in individuals with schizophrenia spectrum disorders (SSDs). However, it remains unclear which specific retinal layers are affected; how the retina, brain, and clinical symptomatology are connected; and how alterations of the visual system are related to genetic disease risk.

METHODS: Optical coherence tomography, electroretinography, and brain magnetic resonance imaging were applied to comprehensively investigate the visual system in a cohort of 103 patients with SSDs and 130 healthy control individuals. The sparse partial least squares algorithm was used to identify multivariate associations between clinical disease phenotype and biological alterations of the visual system. The association of the revealed patterns with individual polygenic disease risk for schizophrenia was explored in a post hoc analysis. In addition, covariate-adjusted case-control comparisons were performed for each individual optical coherence tomography and electroretinography parameter.

RESULTS: The sparse partial least squares analysis yielded a phenotype-eye-brain signature of SSDs in which greater disease severity, longer duration of illness, and impaired cognition were associated with electrophysiological alterations and microstructural thinning of most retinal layers. Higher individual loading onto this disease-relevant signature of the visual system was significantly associated with elevated polygenic risk for schizophrenia. In case-control comparisons, patients with SSDs had lower macular thickness, thinner retinal nerve fiber and inner plexiform layers, less negative a-wave amplitude, and lower b-wave amplitude.

CONCLUSIONS: This study demonstrates multimodal microstructural and electrophysiological retinal alterations in individuals with SSDs that are associated with disease severity and individual polygenic burden.

https://doi.org/10.1016/j.biopsych.2024.04.014

An increasing number of studies indicate retinal alterations in individuals with schizophrenia spectrum disorders (SSDs) (1–3). Based on a common embryonic origin (4,5), the retina shares numerous anatomical and physiological similarities with the brain (6,7). Accordingly, it has been postulated that the retina is an easily accessible window to the brain (6,8).

Unlike the brain, retinal structures can be studied non-invasively in much greater detail, at a resolution of a few micrometers, with the light-based method of optical coherence tomography (OCT) (Figure S1 in Supplement 1) (9). Previous OCT studies of individuals with SSDs provide strong evidence for reduced overall macular thickness (MT) and a thinner peripapillary retinal nerve fiber layer (RNFL) and ganglion cell–inner plexiform layer compared with healthy control participants (HCs), which has also been confirmed in recent meta-analyses (1,2,10,11). However, regarding the effect sizes on MT, RNFL, and ganglion cell–inner plexiform layer and alterations of other retinal layers, the results of previous studies contain some heterogeneity, possibly due to the small sample sizes of many studies and varying sample compositions (e.g., chronic vs. acute disease stages), as well as the heterogeneity of SSDs themselves (2,3,11–20). Moreover, due to technical limitations of the applied OCT technology (21) and image segmentation procedures (22), most previous studies have focused only on total retinal thickness and the thicknesses of the inner retinal layers (2). Meanwhile, advances in OCT

SEE COMMENTARY ON PAGE 769

ISSN: 0006-3223

technology, including the advent of spectral-domain OCT, have enabled reliable segmentation of all individual retinal layers (21). In SSDs, to date only a few low-powered studies with 25 to 35 patients and 15 to 50 HCs have analyzed all retinal layers individually and also indicated alterations of the outer retinal layers, especially the outer nuclear layer (ONL) (23–26). Thus, larger studies are required to confirm which individual retinal layers are particularly affected in SSDs.

Furthermore, recent studies have also indicated electrophysiological alterations of the outer retinal layers in SSDs (3,10,27–34). Electroretinography (ERG) (Figure S1 in Supplement 1) is a well-established tool to study retinal function that measures the electrical response of retinal cells to light stimuli (28). Recent ERG studies in individuals with schizophrenia (SZ) have pointed to a dysfunction of photoreceptors and bipolar cells (27,28,31) that appeared to be partially independent of effects of antipsychotic medication (27,28).

Although there is also evidence for alterations of the visual cortex in psychotic disorders (35), little is known about the extent to which retinal and cerebral alterations in SSDs are intertwined. Few studies have integrated magnetic resonance imaging (MRI) and OCT data in SSDs, suggesting coimpairment of the retina and visual cortex (36–39) as well as a possible link between ONL thinning and reduced total brain and white matter (WM) volumes in patients with psychosis (25).

Moreover, SZ is a disease with a substantial polygenic contribution and an estimated heritability of about 80% (40). Common variants at 287 risk loci have been associated with SZ in the latest genome-wide association study (41). Interestingly, recent studies have identified pleiotropic genetic variants that are associated with both retinal thickness and SZ (42,43). However, genetic investigations at the individual patient level in the field of retinal studies related to SSDs are lacking.

In summary, current evidence points to structural and functional retinal changes in SSDs. However, the etiology of these alterations is still unknown, and most previous studies have focused on either OCT or ERG (10). Thus, multimodal approaches that integrate structural and functional retinal findings as well as neuroimaging and genetics are needed to advance our understanding of retinal alterations in SSDs (10). Moreover, there is a need to assess whether patients with higher disease severity display more pronounced retinal alterations to explore the potential of the retina as a neuroimaging biomarker.

Therefore, in the current study, we performed a comprehensive multimodal analysis of the visual system in a large cross-sectional cohort of patients with SSDs and HCs. We conducted single-layer segmentation of retinal OCT scans as well as ERG and brain MRI and applied a sparse partial least squares (SPLS) algorithm to identify a comprehensive disease signature of SSDs that captures potential associations between disease severity and biological alterations of the visual system. Moreover, we aimed to investigate the association between these patterns and individual polygenic risk for SZ.

METHODS AND MATERIALS

Study Sample and Clinical Assessment

This project was part of the Clinical Deep Phenotyping study (44), an add-on study to the Munich Mental Health Biobank (ethics project No. 18-716) (45) that was approved by the ethics committee of the Faculty of Medicine, Ludwig Maximilian University Munich (project Nos. 20–0528 and 22-0035) and registered at the German Clinical Trials Register (DRKS00024177). It included patients with a diagnosis of SZ, schizoaffective disorder (SZA), or brief psychotic disorder as well as HCs without a history of psychiatric disorders during their lifetime according to the Mini-International Neuropsychiatric Interview (46). Additional study information and detailed inclusion and exclusion criteria are described in Supplemental Methods in Supplement 1. Psychotic symptom severity was assessed with the Positive and Negative Syndrome Scale (PANSS) (47), and cognitive performance was assessed with the Brief Assessment of Cognition in Schizophrenia (BACS) (48). BACS scores were *z*-standardized (Supplemental Methods in Supplement 1). Current antipsychotic medication was converted into chlorpromazine equivalent doses (49). Participants also underwent an eye examination (Supplemental Methods in Supplement 1) to measure refraction, best-corrected visual acuity, and intraocular pressure (IOP).

Optical Coherence Tomography

Macular volume scans were obtained with a ZEISS CIRRUS HD-OCT 5000 device (Carl Zeiss Meditec AG) as previously described (13) (see Supplemental Methods in Supplement 1 for details). In short, scans were segmented by using Iowa Reference Algorithms version 3.8.0 (Retinal Image Analysis Lab) (50–53) to obtain the thicknesses of the RNFL; ganglion cell layer; inner plexiform layer (IPL); inner nuclear layer; outer plexiform layer; combined Henle fiber layer (HFL), ONL, and myoid zone (MZ) of the photoreceptor inner segments (HFL/ONL/MZ); ellipsoid zone; photoreceptor outer segment; interdigitation zone; and retinal pigment epithelium (Figure S1A–C in Supplement 1); thicknesses were measured in each subfield of the ETDRS (Early Treatment Diabetic Retinopathy Study) grid (Figure S1D in Supplement 1). Additionally, the MT and weighted mean layer thicknesses were calculated for the whole ETDRS grid.

Electroretinography

Photopic full-field ERG was performed with a RET*eval* electroretinograph (LKC Technologies, Inc.). The protocol, which was obtained from Demmin *et al.* (28), was provided by Steven Silverstein, University of Rochester Medical Center, Rochester, New York, and is described in detail in Supplemental Methods in Supplement 1. Briefly, the ERG protocol included 3 flash ERG conditions (P_1, P_{PhNR}, P_2) that allowed us to obtain amplitudes and implicit times of a- and b-waves and the corresponding b/a ratio (Figure S1E in Supplement 1). P_1 was a 100 Td·second stimulus presented at 1 Hz without background luminance; P_{PhNR} was a red stimulus presented against a blue background and was included to measure the photopic negative response (PhNR) as a proxy for ganglion cell function; P_2 had the same flash intensity as P_1 but was presented against a white background and at a frequency of 2 Hz. The protocol also included a flicker condition (P_F) to isolate the cone system (54) (Figure S1E in Supplement 1).

Magnetic Resonance Imaging

MRI recordings were performed on a 3T Siemens MAGNETOM Prisma scanner (Siemens Healthineers AG) with a 32-channel head coil. T1-weighted scans were acquired by using a magnetization-prepared rapid acquisition gradient-echo sequence with an isotropic voxel size of 0.8 mm^3, 208 slices, a repetition time of 2500 ms, an echo time of 2.22 ms, a flip angle of 8°, and a field of view of 256 mm^2. Preprocessing and brain volume calculations were performed with NAMNIs version 0.3 software (55). The Jülich Atlas (56) was used to obtain whole-brain gray matter (GM) and WM volumes and the GM and WM volumes of the following regions of interest in the left and right brain hemispheres: visual area 1 (V1; Brodmann area 17), V2 (Brodmann area 18), V3, V4, V5, and lateral geniculate body; volumes were calculated in mm^3 and corrected for intracranial volume. The volumes of the optic nerves were calculated by adding the respective GM and WM volumes. Furthermore, the volume of the optic chiasm was calculated with FreeSurfer (version 6.0; available at: https://surfer.nmr.mgh.harvard.edu/) (57).

Genotyping and Polygenic Risk Score Calculation

Individuals were genotyped using Illumina's Global Screening Array version 3.0 (Life & Brain GmbH). After genotype imputation (Supplemental Methods in Supplement 1), genotype dosage data were used to calculate polygenic risk (i.e., polygenic risk score [PRS]) for SZ (SZ-PRS) for 213 individuals corresponding to the case-control cohort used in this study based on the results of the Psychiatric Genomics Consortium Wave 3 SZ genome-wide association study (41). Posterior single nucleotide polymorphism effect sizes were inferred under continuous shrinkage priors using PRS-CS (58). The global shrinkage parameter (φ) was estimated using a fully Bayesian approach (58).

Statistical Analysis

To capture multivariate associations between phenotypic (i.e., clinical and sociodemographic) and biological (OCT, ERG, MRI) data, we applied an SPLS algorithm (59) to our multimodal cohort of patients with an SSD and HCs as implemented by Popovic *et al.* (60,61). Partial least squares is an unsupervised machine learning method that uses singular value decomposition to identify pairs of weight vectors, i.e., latent variables (LVs); this approach maximizes the covariance between 2 different data views (60). These LVs place weights on the features of 2 different matrices (62), indicating how strongly and in which direction the features are associated with each other in a multivariate context (61). When given phenotypic and biological eye-related data, as in this case, partial least squares identifies signatures between these 2 data domains, thus generating phenotype-eye-brain signatures. SPLS also enforces sparsity on these weight vectors so that only the most relevant features are kept within the signatures (60,61).

For model generation and testing, the SPLS algorithm was embedded in a 5 × 5-fold nested cross-validation framework (60). In brief, hyperparameters were optimized with a 40 × 40-point grid search on the inner CV1 layer. Significance testing of LVs was performed via permutation testing against 5000 permuted datasets on the outer CV2 layer. Feature weight stability was assessed by using 500 bootstrap samples with optimized hyperparameters (63). Detailed information about the SPLS algorithm and machine learning framework is provided in Supplemental Methods in Supplement 1. Individual loadings on the respective weight vectors, i.e., retina-brain and clinical phenotype scores, were compared between HCs and patients with SZA and SZ using Welch's analysis of variance and the Games-Howell post hoc test. Associations between latent scores and the SZ-PRS were assessed by linear regression (controlling for the first 5 multidimensional scaling ancestry components) in 171 cases and controls that survived quality control and were included in the SPLS analysis.

Furthermore, covariate-adjusted case-control comparisons at the level of individual OCT and ERG features were performed with generalized estimation equations (64), which enable the intraindividual correlation between both eyes to be accounted for (65) (Supplemental Methods in Supplement 1). Age, sex, spherical equivalent, IOP, body mass index, diabetes, hypertension, and smoking status were included as covariates.

Finally, the relationship between retinal layer thicknesses and brain volumes in individuals with an SSD was explored with partial Spearman correlation controlling for age and sex (Supplemental Methods in Supplement 1).

RESULTS

Cohort Characteristics

The study sample comprised 103 individuals with an SSD (33% female, age = 39.08 ± 10.48 years, PANSS total score = 49.57 ± 14.58, illness duration = 13.23 ± 8.75 years, chlorpromazine equivalents = 334.58 ± 282.28 mg) and 130 HCs (50% female, age = 33.58 ± 11.85 years) (Table 1). The most common diagnosis among the patients was SZ (72%), followed by SZA (25%) and brief psychotic disorder (3%). The mean duration of untreated psychosis was 24.11 months (SD = 37.39). Most patients (90%) were taking antipsychotic medication. Forty-two percent of patients were in symptomatic remission.

Multivariate Phenotype-Eye-Brain Signature

We applied the SPLS algorithm to capture multivariate disease-relevant patterns of the visual system. The multivariate analysis identified one significant LV, i.e., a pair of weight vectors (Spearman's $\rho = 0.60$; $p < .001$; $N = 184$, $n_{SSD} = 80$; $n_{HC} = 104$) (Figure 1; Table S1 in Supplement 2).

Clinical Phenotype Pattern. Within the vector of the clinical phenotype parameters (Figure 1B), the highest positive weights were found for duration of illness, age, and being affected by an SSD. Chlorpromazine equivalent doses, duration of untreated psychosis, and PANSS scores also received positive weights. Among PANSS subscales, the lowest weight was found for positive symptoms. The greatest negative weight was found for being an unaffected individual, followed by the BACS composite *z* score and BACS subtests. Among BACS subtests, the greatest negative weight was found for verbal memory, followed by the token motor task and symbol coding. Somatic comorbidities and cardiovascular risk factors (body mass index, smoking, diabetes, and hypertension) also

Table 1. Cohort Characteristics

	SSD		HC		
	Mean ± SD or *n* (%)	*n* or n_{eyes}[a]	Mean ± SD or *n* (%)	*n* or n_{eyes}[a]	*p*
Demographic Characteristics					
Age, Years	39.08 ± 10.48	*n* = 103	33.58 ± 11.85	*n* = 130	<.001[b]
Sex, Female:Male (% Female)	34:69 (33%)	–	65:65 (50%)	–	.011[c]
Current Smoking, Yes:No (% Yes)	45:54 (45%)	–	21:109 (16%)	–	<.001[c]
BMI	29.37 ± 6.50	*n* = 102	23.34 ± 3.26	*n* = 130	<.001[b]
Comorbidities					
Diabetes, yes:no (% yes)	10:93 (10%)	–	0:130 (0%)	–	<.001[c]
Hypertension, yes:no (% yes)	33:70 (32%)	–	16:114 (12%)	–	<.001[c]
Eye Examinations					
BCVA	1.13 ± 0.19	n_{eyes} = 199	1.12 ± 0.21	n_{eyes} = 257	.396[b]
IOP, mmHg	13.74 ± 2.59	n_{eyes} = 200	13.26 ± 2.69	n_{eyes} = 258	.055[d]
Spherical Equivalent, Diopter	−1.48 ± 1.64	n_{eyes} = 200	−0.92 ± 1.52	n_{eyes} = 258	<.001[b]
Disease Characteristics					
Duration of Illness, Years	13.23 ± 8.75	*n* = 99	–	–	
Duration of Untreated Psychosis, Months	24.11 ± 37.39	*n* = 49	–	–	
PANSS Positive Symptoms	11.67 ± 4.26	*n* = 103	–	–	
PANSS Negative Symptoms	12.16 ± 5.03	*n* = 103	–	–	
PANSS General Symptoms	25.93 ± 7.47	*n* = 103	–	–	
PANSS Total Score	49.57 ± 14.58	*n* = 103	–	–	
BACS Composite *z* Score	−1.40 ± 1.28	*n* = 94	0 ± 1.00	*n* = 116	<.001[d]
CPZeq, mg	334.58 ± 282.28	*n* = 94	–	–	
Remission, yes:no (% yes)	43:60 (42%)	–	–	–	
Diagnosis—DSM-5					
Schizophrenia	74 (72%)	–	–	–	
Schizoaffective disorder	26 (25%)	–	–	–	
Brief psychotic disorder	3 (3%)	–	–	–	
Available Data					
OCT	–	*n* = 98, n_{eyes} = 185	–	*n* = 128, n_{eyes} = 250	–
ERG	–	*n* = 102, n_{eyes} = 198	–	*n* = 125, n_{eyes} = 246	–
MRI	–	*n* = 79	–	*n* = 112	–

BACS, Brief Assessment of Cognition in Schizophrenia; BCVA, best-corrected visual acuity; BMI, body mass index; CPZeq, chlorpromazine equivalent dose; ERG, electroretinography; HC, healthy control participant; IOP, intraocular pressure; MRI, magnetic resonance imaging; OCT, optical coherence tomography; PANSS, Positive and Negative Syndrome Scale; SSD, schizophrenia spectrum disorder.

[a]*n* is number of participants; n_{eyes} is number of eyes.

[b]Mann-Whitney *U* test.

[c]Fisher's exact test.

[d]Welch's *t* test.

received smaller positive weights. The lowest weight was found for sex.

Retina-Brain Pattern. The highest weights within the retina-brain vector were found for ERG features, especially b-wave implicit times. Apart from the thickness of the interdigitation zone and the photoreceptor outer segment, the thicknesses of all retinal layers were part of the retina-brain pattern: the right and left IPL thickness received the greatest (negative) weights, followed by the MT, RNFL, and HFL/ONL/MZ thickness. Fourteen of 29 MRI features that covered the visual pathway within the brain were part of the disease signature, but these brain volume features had a much lower weighting than the retinal features.

To address whether the identified phenotype-eye-brain signature in SSD differed between SSD subgroups, we compared the individual loadings between HC, SZA, and SZ groups and found significant differences between the HC and SZA as well as HC and SZ groups for both the clinical phenotype and the retina-brain scores, but no differences were found between SZA and SZ for either one (Figure S2 in Supplement 1; Table S2 in Supplement 2).

Individual Disease Pattern of the Visual System Is Correlated With Genetic Risk

Next, we aimed to investigate the potential connection between the SSD-relevant signature of the visual system and the underlying

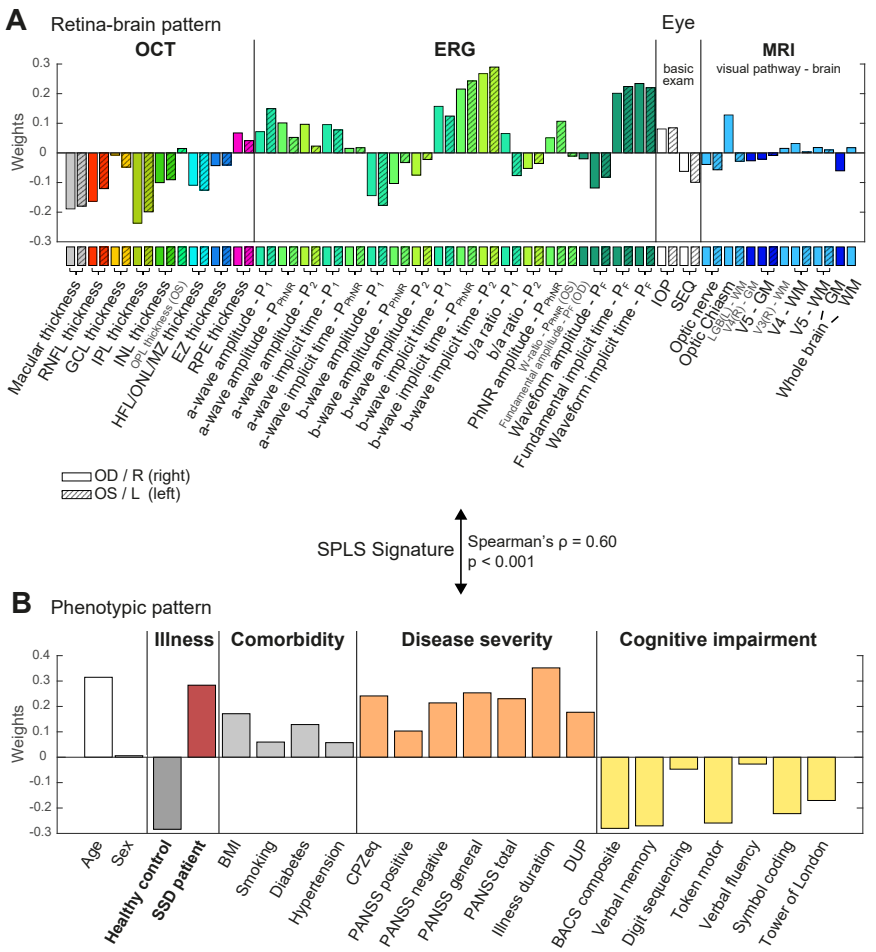

Figure 1. Multidimensional phenotype-eye-brain signature as identified by the sparse partial least squares algorithm (SPLS). Illustration of **(A)** the biological (eye-related) vector and **(B)** the phenotypic vector of the identified latent variable (Spearman's $\rho = 0.60$; $p < .001$; $N = 184$, $n_{SSD} = 80$, $n_{HC} = 104$). The bars visualize the direction and values of the weights assigned to the relevant features incorporated into the latent variable by the SPLS algorithm. Data of the right eye (R) (OD) and left eye (L) (OS) are presented separately; the latter are shown in a hatched pattern. Features where the weight of only one eye was included in the latent variable are written in a thinner, light gray font. BACS, Brief Assessment of Cognition in Schizophrenia; BMI, body mass index; CPZeq, chlorpromazine equivalent dose; DUP, duration of untreated psychosis; ERG, electroretinography; EZ, ellipsoid zone; GCL, ganglion cell layer; GM, gray matter; HC, healthy control participant; HFL, Henle fiber layer; INL, inner nuclear layer; IOP, intraocular pressure; IPL, inner plexiform layer; MRI, magnetic resonance imaging; MZ, myoid zone; OCT, optical coherence tomography; ONL, outer nuclear layer; OPL, outer plexiform layer; PANSS, Positive and Negative Syndrome Scale; PhNR, photopic negative response; RNFL, retinal nerve fiber layer; RPE, retinal pigment epithelium; SEQ, spherical equivalent; SSD, schizophrenia spectrum disorder; WM, white matter.

genetic component of the disease. This was done to investigate whether the identified retina-brain pattern is influenced not only by mediators such as enriched comorbidities but also by the underlying disease biology. Linear regression revealed a significant association of the SZ-PRS with a higher individual loading on the retina-brain vector as well as a higher loading on the clinical phenotype vector (both $p < .001$; $n = 171$) (Figure 2; Table S3 in Supplement 2).

Pronounced Thinning of the Inner Retinal Layers

To provide estimates of between-group differences, we performed additional covariate-adjusted case-control comparisons. Generalized estimation equations were used to compare the MT and the thicknesses of 10 different retinal layers between patients and HCs (Figure 3A; Tables S4–S6 in Supplement 2). The analysis revealed reduced total macular (estimate [95% CI] = −5.81 μm [−9.97 to −1.66]; $q = .034$, where q is the false discovery rate–adjusted p value), RNFL (estimate [95% CI] = −1.49 μm [−2.64 to −0.34]; $q = .04$), and IPL (estimate [95% CI] = −1.36 μm [−2.30 to −0.43]; $q = .034$) thickness in SSD.

To explore whether the observed alterations followed a specific spatial pattern or differed between the right and left eye, we performed subsequent analyses for the different subfields of the ETDRS grid in layers that were significantly altered in SSDs (Figure 3B; Tables S7 and S8 in Supplement 2). Thinning was slightly more pronounced in the nasal than the temporal subfields and almost symmetrical between both eyes. Only for IPL, we found discrete interactions between group and eye that indicated slightly stronger effects of SSDs in the central and inner subfields of the right eye.

Altered Retinal Electrophysiology in SSDs

Consistent with the structural post hoc analysis, we conducted a covariate-adjusted direct case-control comparison with the electrophysiological retinal parameters. For P_1, the a-wave amplitude was significantly less negative (estimate [95% CI] = 5.08 μV [2.64 to 7.52]; $q = .001$), and the b-wave amplitude was significantly less positive (estimate [95% CI] = −7.40 μV [−11.43 to −3.38]; $q = .003$) in patients with an SSD than in HCs (Figure 4; Tables S9–S11 in Supplement 2).

Relationship Between Altered Retinal Layers and Downstream Visual Regions

To explore potential direct retina-brain associations and to evaluate whether the retina can in fact be considered a window

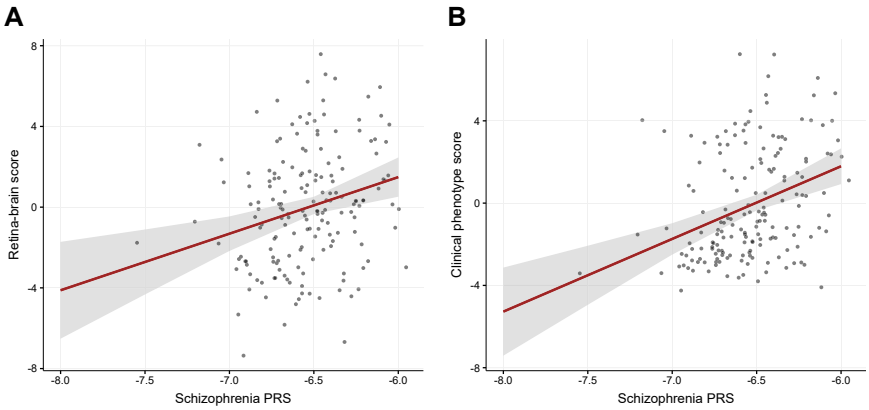

Figure 2. Significant association between polygenic risk for schizophrenia and individual loadings on the phenotype-eye-brain signature. **(A)** Association between schizophrenia polygenic risk scores (PRSs) and retina-brain scores (R^2_{adj} = 0.058, $p < .001$). **(B)** Association between schizophrenia-PRSs and clinical phenotype scores (R^2_{adj} = 0.109, $p < .001$). n = 171. Red lines represent the predicted values as obtained from linear regression models; gray area indicates the 95% CI; points represent the raw data.

to the brain, we calculated partial Spearman correlations between retinal layers that were altered in SSDs and downstream (sub)cortical structures of the visual pathway as well as whole-brain volume within patients with an SSD. The highest correlations were found between RNFL thickness and volumes of the right (ρ = 0.37) and left (ρ = 0.29) optic nerves, but they were not statistically significant after false discovery rate adjustment. All other examined retina-brain connections were weaker and not significant (Figure S3 in Supplement 1; Table S12 in Supplement 2).

DISCUSSION

This study provides evidence of both microstructural and electrophysiological alterations in the visual system among individuals with an SSD that are more pronounced in patients with greater disease severity. Moreover, we have established a relationship between the degree of individual disease-associated alterations of the visual system and the polygenic burden for SZ.

The applied SPLS analysis revealed a multivariate phenotype-eye-brain signature of SSDs, linking phenotypic features of chronic disease and greater disease severity (such as longer duration of illness, higher PANSS sores, higher chlorpromazine equivalent doses, and impaired cognition) to altered retinal markers (such as prolonged latencies and reduced amplitudes of ERG responses and microstructural thinning of retinal layers) and discrete changes in visual cortical areas. The multimodal retina-brain pattern was characterized by thinning of several retinal layers, with the IPL, the RNFL, and the HFL/ONL/MZ being most affected. Moreover, the signature implicated alterations of electrophysiological markers related to bipolar cell function, specifically longer b-wave implicit times, and photoreceptor function (66), consistent with the findings of previous case-control studies (27,28,31). Notably, there were no significant differences between SZ and SZA in the loadings onto the weight vectors, indicating that the revealed signature is not exclusive to a particular subgroup but rather reflects a broader phenotype of SSDs (10,67). Consistent with these results, the additional case-control OCT analysis confirmed RNFL and IPL thinning in SSDs that was nearly symmetrical in both eyes, indicating a general biological effect of microstructural alterations of retinal ganglion cell (RGC) axons in the RNFL and altered synaptic connections or branching of bipolar cells, RGCs, or amacrine cells in the IPL (68). The effects were more nasally than temporally pronounced, which may indicate that retinal alterations in SSDs are more evident within the maculopapular bundle.

The ERG investigation uncovered distinct electrophysiological alterations, i.e., lower a- and b-wave amplitudes in SSDs, indicating reduced photoreceptor and bipolar cell responses to light stimuli in SSDs (66). However, while lower HFL/ONL/MZ thickness had a comparatively high weight in the multivariate signature, the covariate-adjusted direct case-control comparison did not identify significant group-level differences in the thicknesses of the outer retinal layers or the inner nuclear layer, where the somata of photoreceptors and bipolar cells are located (68). Thus, HFL/ONL/MZ thickness could be especially affected in patients with greater disease severity. Moreover, functional changes may become apparent earlier in the course of the diseases than morphological alterations, as has been described in eye conditions such as glaucoma (69). Another (technical) hypothesis that could partially address the discrepancy between structural and functional findings is that the applied full-field ERG assesses general retinal function (54) while our OCT protocol only covered the macular center of the retina.

Previous studies have reported both reduced (26,28) and increased (32) PhNR amplitudes in SSDs, indicating potential electrophysiological alterations of RGCs (66,70–72). In partial contrast to these findings, in the current well-powered study, while we observed RNFL thinning indicative of RGC axonal loss, no significant group effect of SSD on the PhNR, the W-ratio, or the ganglion cell layer [where the RGC somata are located (68)] was found. Additionally, apart from RNFL thickness, RGC-related parameters received only low weights in the multivariate signature.

A topic of lively discussion is whether retinal changes in SSDs originate primarily in the retina itself as a result of unknown disease-driven mechanisms, are a consequence of retrograde transsynaptic degeneration (3,73), or are mediated by other variables that are enriched in individuals with SSDs, such as cardiovascular risk factors

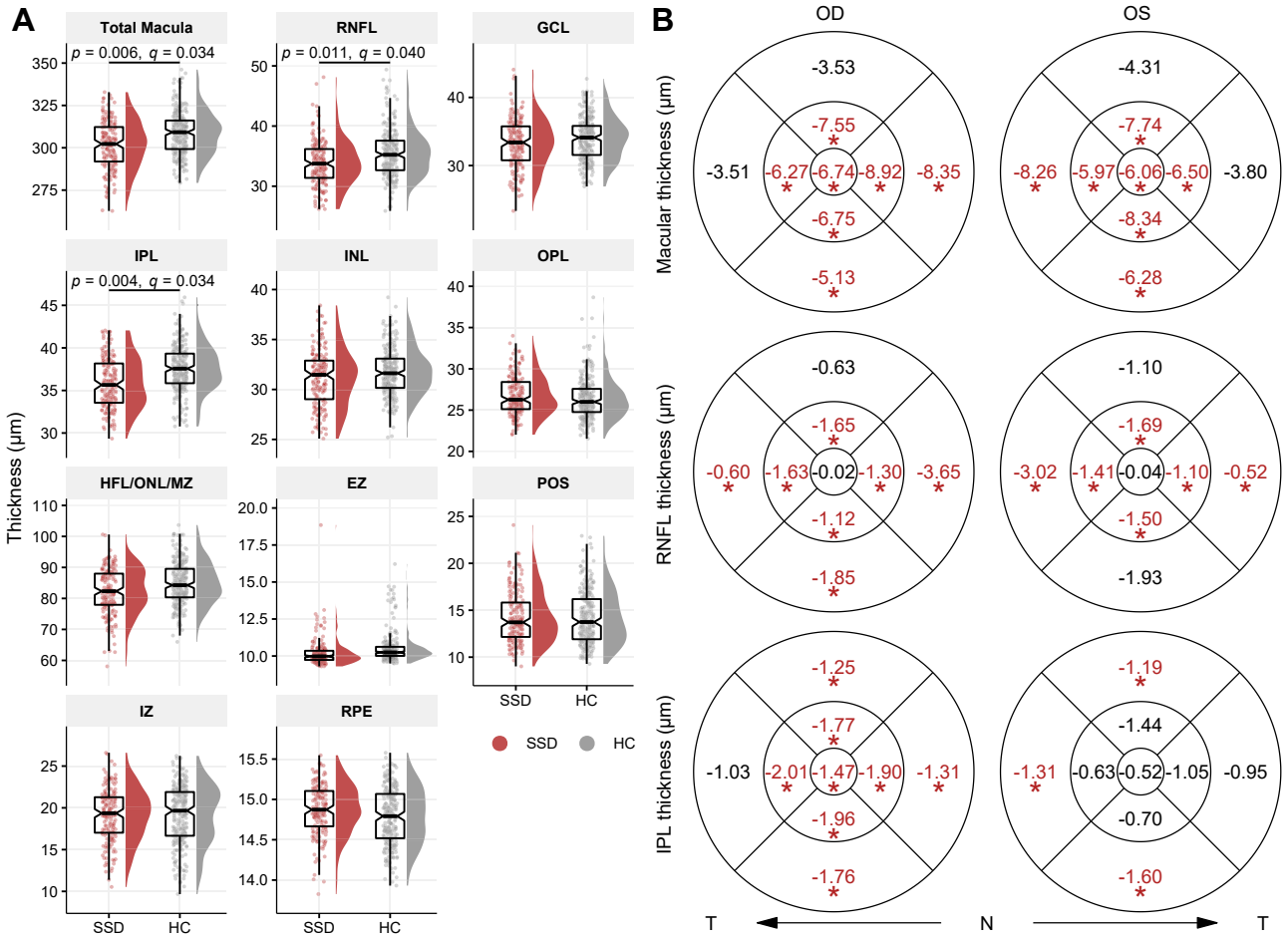

Figure 3. Thinner retinal layers in schizophrenia spectrum disorders (SSDs) as shown by optical coherence tomography. **(A)** Comparison of mean thicknesses of retinal layers in the whole 6-mm-diameter area of the ETDRS (Early Treatment Diabetic Retinopathy Study) grid between the healthy control (HC) group (gray) and individuals with SSDs (red), illustrated by combined box, density, and scatterplots. Shown are the total macular thickness ($q = .034$, where q is the false discovery rate–adjusted p value) and the following layers: retinal nerve fiber layer (RNFL) ($q = .04$), ganglion cell layer (GCL) ($q = .439$), inner plexiform layer (IPL) ($q = .034$), inner nuclear layer (INL) ($q = .614$), outer plexiform layer (OPL) ($q = .614$), combined Henle fiber layer (HFL)/outer nuclear layer (ONL)/myoid zone (MZ) ($q = .142$), ellipsoid zone (EZ) ($q = .439$), photoreceptor outer segment (POS) ($q = .614$), interdigitation zone (IZ) ($q = .614$), and retinal pigment epithelium (RPE) ($q = .614$). Data points represent individual eyes. Groups were compared with generalized estimation equations to control for age, sex, spherical equivalent, intraocular pressure, body mass index, diabetes, hypertension, and smoking status. n is number of participants, n_{eyes} is number of eyes: $n_{SSD} = 96$, $n_{eyes\_SSD} = 182$, $n_{HC} = 128$, $n_{eyes\_HC} = 250$. *$q < .05$. **(B)** Maps of the right eye (OD) and left eye (OS) depicting the marginal effect of SSD in µm on each subfield of the ETDRS grid in overall macular thickness, RNFL, and IPL, as obtained with generalized estimation equations to control for age, sex, spherical equivalent, intraocular pressure, body mass index, diabetes, hypertension, smoking status, eye, and including an interaction between eye and group. Statistically significant effects are highlighted in red. $n_{SSD} = 96$, $n_{eyes\_SSD} = 182$, $n_{HC} = 128$, $n_{eyes\_HC} = 250$. *$p < .05$. N, nasal; T, temporal.

(3,13,74–78). In the current study, we identified several microstructural and electrophysiological alterations of the retina in SSDs that were highly robust even though we controlled for a series of covariates associated with retinal thickness, such as age, sex, spherical equivalent, IOP, body mass index, diabetes, hypertension, and smoking (3,79,80). However, there remains a possibility that other (environmental) factors could partially mediate the observed retinal thinning. For example, social deprivation has been shown to be associated with thinner inner retinal layers in the general population (81).

Post hoc analyses revealed no statistically significant correlations between altered retinal structures and downstream visual regions or total GM or WM volume in patients (Figure S3 in Supplement 1), indicating that structural retinal alterations in SSDs are not directly reflected by structural changes of the brain. These findings challenge the hypothesis that the observed retinal thinning is mainly due to retrograde processes in the classic visual pathway, such as transsynaptic degeneration. Instead, retinal and cerebral changes in SSDs may occur independently but be due to common, as yet unknown mechanisms (1).

Given the recent evidence of genetic pleiotropy between retinal thickness and SZ (42,43), the observation of IPL thinning also in unaffected first-degree relatives of patients with SZ (82), and the fact that electroretinographic alterations have also been described in offspring of individuals diagnosed with SZ and other psychiatric diseases (83–86), how the observed alterations of the visual system in SSDs relate to the polygenic architecture of the diseases was an important question.

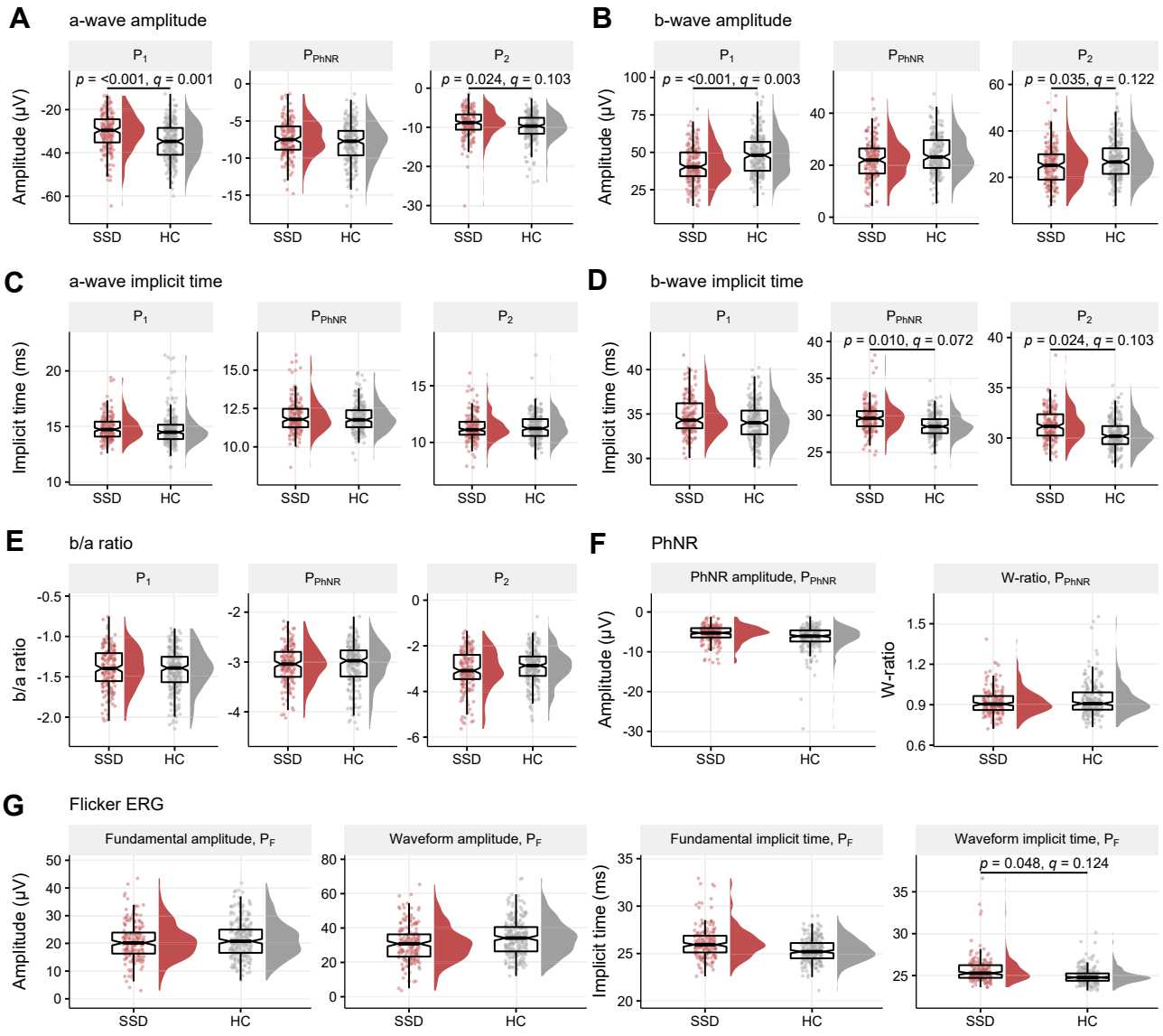

Figure 4. Altered photoreceptor and bipolar cell responses in schizophrenia spectrum disorders (SSDs). Comparison of electroretinography (ERG) measures between patients with SSDs and healthy control participants (HCs) for 4 photopic conditions (*n* is number of participants, n_{eyes} is number of eyes: P_1: n_{SSD} = 96, n_{eyes_SSD} = 182, n_{HC} = 124, n_{eyes_HC} = 241; P_{PhNR}: n_{SSD} = 92, n_{eyes_SSD} = 176, n_{HC} = 118, n_{eyes_HC} = 219; P_2: n_{SSD} = 98, n_{eyes_SSD} = 178, n_{HC} = 123, n_{eyes_HC} = 228; and P_F: n_{SSD} = 97, n_{eyes_SSD} = 185, n_{HC} = 125, n_{eyes_HC} = 246), illustrated with combined box, density, and scatterplots. Shown are **(A)** a-wave and **(B)** b-wave amplitudes, **(C)** a-wave and **(D)** b-wave implicit times, and **(E)** the b/a ratio (quotient of the b- and a-wave amplitudes) for P_1, P_{PhNR}, and P_2; **(F)** the photopic negative response (PhNR) amplitudes (left) and the W-ratio (right) for P_{PhNR}; and **(G)** both the underlying fundamental and the reconstructed waveform implicit times (left) and amplitudes (right) in the flicker ERG test (P_F). Data points represent individual eyes. *$q < .05$ (where *q* is the false discovery rate–adjusted *p* value). *p* Values were obtained with generalized estimation equations to control for age, sex, spherical equivalent, intraocular pressure, body mass index, diabetes, hypertension, and smoking status. Measures in patients with SSDs are shown in red, and measures in HCs are shown in gray.

Fascinatingly, our genetic analysis uncovered an association between individual loadings on the retina-dominated visual system signature and individual polygenetic risk for SZ. Although these findings do not allow for causal conclusions to be drawn, they indicate that retinal alterations in SSDs are influenced to some extent by unidentified genetically driven mechanisms of the complex polygenic disease. Notably, the SZ-PRS explained only a small part of the variance in retina-brain scores (Figure 2). Consistent with the multifactorial etiology of SSDs (67,87,88), nongenetic risk factors are likely also implicated in the pathophysiological processes that drive alterations in retinal structure and function in SSDs.

This study has several limitations. First, an additional effect of antipsychotics on the retina cannot be excluded. For example, flash ERG responses in healthy volunteers were altered after intake of antipsychotic medications (89–94). However, the significant link between the SZ-PRS and the individual loadings on the revealed visual system signature

strongly argues against an effect solely of medical treatment and supports the hypothesis that, at least in part, primary disease mechanisms affect retinal structure and function in SSDs. Second, because of its cross-sectional nature, the current study does not provide direct evidence about the longitudinal development and stability of retinal alterations in SSDs. Third, the specificity of the observed retinal alterations in SSDs should be addressed in future studies that include individuals with other psychiatric diagnoses. Fourth, there may be nonmonotonic relationships between some clinical features and retinal alterations (18) that were not captured by the SPLS algorithm. Fifth, the comparability of our results with previous OCT studies may be limited by our use of a different segmentation algorithm that combined the ONL and the MZ of the inner segments into a single layer. Sixth, although the applied handheld ERG is far more feasible in clinical research settings, and noninvasive skin electrodes are better accepted by study participants, conventional devices using corneal electrodes have a better signal-to-noise ratio (95) and may therefore be more sensitive to subtle changes.

Conclusions

Our study provides evidence that microstructural and functional alterations of the retina in SSDs are associated with disease duration and severity as well as with individual genetic disease risk. Therefore, our findings indicate that retinal alterations in SSDs have both state and trait (10) aspects. Moreover, the revealed association with genetic risk for SZ highlights the potential of retinal alterations as an endophenotype candidate in SSDs (67). In this regard, as an accessible part of the central nervous system, the retina may contribute to a better understanding of the neurobiological mechanisms of SSDs. Apart from scientific applications, it remains to be investigated to what extent retinal neuroimaging and electrophysiology could complement established investigations in clinical settings, for example, for subgroup identification or as a cost-effective screening tool for central nervous system alterations over time.

ACKNOWLEDGMENTS AND DISCLOSURES

EB, VG, and PP were supported by doctoral scholarships from the Faculty of Medicine, Ludwig Maximilian University (LMU) Munich, Munich, Germany. DP and FJR were supported by the Else Kröner-Fresenius Foundation (Research College "Translational Psychiatry") for their Residency/Ph.D. track at the International Max Planck Research School for Translational Psychiatry, Munich, Germany. FJR and ECS were supported by the Munich Clinician Scientist Program of the Faculty of Medicine, LMU Munich, Munich, Germany (Grant Nos. FöFoLe 009/2019 and Advanced Track 01/2021, respectively). FJR received funding from the Lisa Oehler-Stiftung (Grant No. 2022–2024) and the B. Braun-Stiftung (Grant No. BBST-D-20-00032). EW was supported by the Förderprogramm für Forschung und Lehre, University Hospital, LMU Munich (registration No. 1083). PF and AH were supported by the Federal Ministry of Education and Research (Bundesministerium für Bildung und Forschung) within the initial phase of the German Center for Mental Health (Grant Nos. FKZ 01EE2303A and 01EE2303F [to PF] and FKZ 01EE2303C [to AH]). PF, GH, and VY received funding from the Bundesministerium für Bildung und Forschung within the Era-Net Neuron project GDNF_UpReg (Grant No. FKZ 01EW2206). The procurement of the MRI scanner was supported by the German Research Foundation (Deutsche Forschungsgemeinschaft) grant for major research (DFG, INST 86/1739-1 FUGG).

DK, FJR, and EW led the general design and conceptualization of and AH, PF, AS, and OP supervised the Munich Clinical Deep Phenotyping study. The current study was conceptualized by EB, VG, DP, and FJR. JM, EW, and VY trained staff in diagnostic and clinical assessments. Eye examinations were performed by EB, VG, and PP under the ophthalmologic supervision of CK, SPr, and BS. MRI acquisition and processing were performed by GH and LR. Genotyping and genetic analysis were conducted by SPa, FJR, ECS, and VY. SPLS analysis was performed by DP. All other statistical analyses were performed by EB. Data visualization was performed by EB, VG, DP, FJR, and SX. EB, VG, and FJR wrote the first draft of the manuscript. All authors contributed to and approved the final version of the manuscript. FJR supervised the work.

We thank all participants for their support. Furthermore, we thank all researchers and clinical and administrative staff from the Departments of Ophthalmology and Psychiatry and Psychotherapy at the University Hospital, LMU Munich, Munich, Germany for their help conducting this study; Steven Silverstein, University of Rochester Medical Center, Rochester, New York, who provided the electroretinography protocol; and Jacquie Klesing, B.Med.Sci. (Hons.), Board-certified Editor in the Life Sciences, for editing assistance with the manuscript.

The deidentified data of this study are available in the Zenodo repository at https://doi.org/10.5281/zenodo.7510469.

AH received speaker fees from AbbVie, Advanz, Janssen, Otsuka, Lundbeck, Rovi, and Recordati and was a member of the advisory boards of these companies and Boehringer Ingelheim. BS received speaker fees from Novartis Pharma GmbH. CK received speaker fees from Bayer AG and received grants from Zeiss Meditech outside the submitted work. EW was a member of the advisory boards of Boehringer Ingelheim and Recordati. OP received speaker fees from Lundbeck, Otsuka, Takeda, and Janssen and was a member of the advisory boards of Lundbeck and Janssen. PF received speaker fees from Boehringer Ingelheim, Janssen, Otsuka, Lundbeck, Recordati, and Richter and was a member of the advisory boards of these companies and Rovi. SPr received honoraria from Novartis Pharma GmbH, Pharm Allergan, Zeiss, BVI, Bayer, Alcon, B&L, and Roche and was a member of the advisory boards of these companies. He served as a consultant for Zeiss, BVI, B&L, and Roche. All other authors report no biomedical financial interests or potential conflicts of interest.

ARTICLE INFORMATION

From the Department of Psychiatry and Psychotherapy, LMU University Hospital, LMU Munich, Munich, Germany (EB, VG, DP, PP, VY, LR, GH, SX, JM, OP, PF, AS, CDP Working Group, DK, FJR); Max Planck Institute of Psychiatry, Munich, Germany (EB, DP, SPa, PF, AS, CDP Working Group, FJR); International Max Planck Research School for Translational Psychiatry, Munich, Germany (VY); Institute of Psychiatric Phenomics and Genomics, LMU Munich, Munich, Germany (SPa, ECS); NeuroImaging Core Unit Munich, LMU University Hospital, LMU Munich, Munich, Germany (LR, DK); Evidence-Based Psychiatry and Psychotherapy, Faculty of Medicine, University of Augsburg, Augsburg, Germany (GH, CDP Working Group, EW); Department of Ophthalmology, LMU University Hospital, LMU Munich, Munich, Germany (SPr, CK, BS); Institute of Human Genetics, University Hospital, Faculty of Medicine, University of Bonn, Bonn, Germany (ECS); Department of Psychiatry and Psychotherapy, University Hospital, Faculty of Medicine, University of Bonn, Bonn, Germany (ECS); Department of Psychiatry, Psychotherapy, and Psychosomatics, Faculty of Medicine, University of Augsburg, Augsburg, Germany (AH, CDP Working Group, EW); German Center for Mental Health, partner site Munich-Augsburg, Germany (AH, PF, AS); Laboratory of Neurosciences (LIM-27), Institute of Psychiatry, University of São Paulo, São Paulo, Brazil (AS); and Munich Center for Neurosciences, LMU Munich, Planegg-Martinsried, Germany (DK).

CDP Working Group: Valéria de Almeida, Stephanie Behrens, Emanuel Boudriot, Mattia Campana, Fanny Dengl, Peter Falkai, Laura E. Fischer, Nadja Gabellini, Vanessa Gabriel, Thomas Geyer, Katharina Hanken, Alkomiet Hasan, Genc Hasanaj, Georgios Ioannou, Iris Jäger, Sylvia de Jonge, Temmuz Karali, Susanne Karch, Berkhan Karslı, Daniel Keeser, Christoph Kern, Nicole Klimas, Lenka Krčmář, Julian Melcher, Matin Mortazavi, Joanna Moussiopoulou, Karin Neumeier, Frank Padberg, Boris Papazov, Sergi Papiol, Pauline Pingen, Oliver Pogarell, Siegfried Priglinger, Florian J. Raabe, Lukas Roell, Moritz J. Rossner, Andrea Schmitt, Susanne Schmölz, Enrico

Schulz, Benedikt Schworm, Elias Wagner, Sven Wichert, Vladislav Yakimov, Peter Zill (collaborators listed alphabetically). Main contact: Florian J. Raabe, Department of Psychiatry and Psychotherapy, LMU University Hospital, LMU Munich, Munich, Germany.

EB and VG contributed equally to this work.

Address correspondence to Florian J. Raabe, M.D., Ph.D., at florian.raabe@med.uni-muenchen.de.

Received Aug 3, 2023; revised Mar 30, 2024; accepted Apr 14, 2024.

Supplementary material cited in this article is available online at https://doi.org/10.1016/j.biopsych.2024.04.014.

REFERENCES

1. Gonzalez-Diaz JM, Radua J, Sanchez-Dalmau B, Camos-Carreras A, Zamora DC, Bernardo M (2022): Mapping retinal abnormalities in psychosis: Meta-analytical evidence for focal peripapillary and macular reductions. Schizophr Bull 48:1194–1205.
2. Komatsu H, Onoguchi G, Jerotic S, Kanahara N, Kakuto Y, Ono T, *et al.* (2022): Retinal layers and associated clinical factors in schizophrenia spectrum disorders: A systematic review and meta-analysis. Mol Psychiatry 27:3592–3616.
3. Silverstein SM, Fradkin SI, Demmin DL (2020): Schizophrenia and the retina: Towards a 2020 perspective. Schizophr Res 219:84–94.
4. Heavner W, Pevny L (2012): Eye development and retinogenesis. Cold Spring Harb Perspect Biol 4:a008391.
5. Sadler TW (2018): Eye. In: Langman's Medical Embryology, 14th ed. Philadelphia, PA: Wolters Kluwer, 360–369.
6. London A, Benhar I, Schwartz M (2013): The retina as a window to the brain-from eye research to CNS disorders. Nat Rev Neurol 9:44–53.
7. Marchesi N, Fahmideh F, Boschi F, Pascale A, Barbieri A (2021): Ocular neurodegenerative diseases: Interconnection between retina and cortical areas. Cells 10:2394.
8. Schönfeldt-Lecuona C, Kregel T, Schmidt A, Pinkhardt EH, Lauda F, Kassubek J, *et al.* (2016): From imaging the brain to imaging the retina: Optical coherence tomography (OCT) in schizophrenia. Schizophr Bull 42:9–14.
9. Aumann S, Donner S, Fischer J, Müller F (2019): Optical coherence tomography (OCT): Principle and technical realization. In: Bille JF, editor. High Resolution Imaging in Microscopy and Ophthalmology: New Frontiers in Biomedical Optics. Cham, Switzerland: Springer International Publishing, 59–85.
10. Komatsu H, Onoguchi G, Silverstein SM, Jerotic S, Sakuma A, Kanahara N, *et al.* (2024): Retina as a potential biomarker in schizophrenia spectrum disorders: A systematic review and meta-analysis of optical coherence tomography and electroretinography. Mol Psychiatry 29:464–482.
11. Wagner SK, Cortina-Borja M, Silverstein SM, Zhou Y, Romero-Bascones D, Struyven RR, *et al.* (2023): Association between retinal features from multimodal imaging and schizophrenia. JAMA Psychiatry 80:478–487.
12. Domagała A, Domagała L, Kopiś-Posiej N, Harciarek M, Krukow P (2023): Differentiation of the retinal morphology aging trajectories in schizophrenia and their associations with cognitive dysfunctions. Front Psychiatry 14:1207608.
13. Boudriot E, Schworm B, Slapakova L, Hanken K, Jäger I, Stephan M, *et al.* (2023): Optical coherence tomography reveals retinal thinning in schizophrenia spectrum disorders. Eur Arch Psychiatry Clin Neurosci 273:575–588.
14. Lee WW, Tajunisah I, Sharmilla K, Peyman M, Subrayan V (2013): Retinal nerve fiber layer structure abnormalities in schizophrenia and its relationship to disease state: Evidence from optical coherence tomography. Invest Ophthalmol Vis Sci 54:7785–7792.
15. Blose BA, Lai A, Crosta C, Thompson JL, Silverstein SM (2023): Retinal neurodegeneration as a potential biomarker of accelerated aging in schizophrenia spectrum disorders. Schizophr Bull 49:1316–1324.
16. Lai A, Crosta C, Loftin M, Silverstein SM (2020): Retinal structural alterations in chronic versus first episode schizophrenia spectrum disorders. Biomark Neuropsychiatry 2:100013.
17. Ascaso FJ, Rodriguez-Jimenez R, Cabezón L, López-Antón R, Santabárbara J, De la Cámara C, *et al.* (2015): Retinal nerve fiber layer and macular thickness in patients with schizophrenia: Influence of recent illness episodes. Psychiatry Res 229:230–236.
18. Alizadeh M, Delborde Y, Ahmadpanah M, Seifrabiee MA, Jahangard L, Bazzazi N, Brand S (2021): Non-linear associations between retinal nerve fibre layer (RNFL) and positive and negative symptoms among men with acute and chronic schizophrenia spectrum disorder. J Psychiatr Res 141:81–91.
19. Wolfers T, Doan NT, Kaufmann T, Alnæs D, Moberget T, Agartz I, *et al.* (2018): Mapping the heterogeneous phenotype of schizophrenia and bipolar disorder using normative models. JAMA Psychiatry 75:1146–1155.
20. Kango A, Grover S, Gupta V, Sahoo S, Nehra R (2023): A comparative study of retinal layer changes among patients with schizophrenia and healthy controls. Acta Neuropsychiatr 35:165–176.
21. Petzold A, Balcer LJ, Calabresi PA, Costello F, Frohman TC, Frohman EM, *et al.* (2017): Retinal layer segmentation in multiple sclerosis: A systematic review and meta-analysis. Lancet Neurol 16:797–812.
22. Oberwahrenbrock T, Traber GL, Lukas S, Gabilondo I, Nolan R, Songster C, *et al.* (2018): Multicenter reliability of semiautomatic retinal layer segmentation using OCT. Neurol Neuroimmunol Neuroinflamm 5:e449.
23. Samani NN, Proudlock FA, Siram V, Suraweera C, Hutchinson C, Nelson CP, *et al.* (2018): Retinal layer abnormalities as biomarkers of schizophrenia. Schizophr Bull 44:876–885.
24. Schönfeldt-Lecuona C, Kregel T, Schmidt A, Kassubek J, Dreyhaupt J, Freudenmann RW, *et al.* (2020): Retinal single-layer analysis with optical coherence tomography (OCT) in schizophrenia spectrum disorder. Schizophr Res 219:5–12.
25. Bannai D, Lizano P, Kasetty M, Lutz O, Zeng V, Sarvode S, *et al.* (2020): Retinal layer abnormalities and their association with clinical and brain measures in psychotic disorders: A preliminary study. Psychiatry Res Neuroimaging 299:111061.
26. Friedel EBN, Hahn HT, Maier S, Küchlin S, Reich M, Runge K, *et al.* (2022): Structural and functional retinal alterations in patients with paranoid schizophrenia. Transl Psychiatry 12:402.
27. Hébert M, Mérette C, Gagné AM, Paccalet T, Moreau I, Lavoie J, Maziade M (2020): The electroretinogram may differentiate schizophrenia from bipolar disorder. Biol Psychiatry 87:263–270.
28. Demmin DL, Davis Q, Roché M, Silverstein SM (2018): Electroretinographic anomalies in schizophrenia. J Abnorm Psychol 127:417–428.
29. Balogh Z, Benedek G, Kéri S (2008): Retinal dysfunctions in schizophrenia. Prog Neuropsychopharmacol Biol Psychiatry 32:297–300.
30. Warner R, Laugharne J, Peet M, Brown L, Rogers N (1999): Retinal function as a marker for cell membrane omega-3 fatty acid depletion in schizophrenia: A pilot study. Biol Psychiatry 45:1138–1142.
31. Hébert M, Mérette C, Paccalet T, Émond C, Gagné AM, Sasseville A, Maziade M (2015): Light evoked potentials measured by electroretinogram may tap into the neurodevelopmental roots of schizophrenia. Schizophr Res 162:294–295.
32. Moghimi P, Torres Jimenez N, McLoon LK, Netoff TI, Lee MS, MacDonald A 3rd, Miller RF (2020): Electoretinographic evidence of retinal ganglion cell-dependent function in schizophrenia. Schizophr Res 219:34–46.
33. Bernardin F, Schwitzer T, Schwan R, Angioi-Duprez K, Ligier F, Bourion-Bedes S, *et al.* (2022): Altered central vision and amacrine cells dysfunction as marker of hypodopaminergic activity in treated patients with schizophrenia. Schizophr Res 239:134–141.
34. Bernardin F, Schwitzer T, Angioi-Duprez K, Giersch A, Jansen C, Schwan R, Laprevote V (2020): Retinal ganglion cells dysfunctions in schizophrenia patients with or without visual hallucinations. Schizophr Res 219:47–55.
35. Türközer HB, Lizano P, Adhan I, Ivleva EI, Lutz O, Zeng V, *et al.* (2022): Regional and sex-specific alterations in the visual cortex of individuals with psychosis spectrum disorders. Biol Psychiatry 92:396–406.
36. Zhuo C, Ji F, Xiao B, Lin X, Chen C, Jiang D, *et al.* (2020): Antipsychotic agent-induced deterioration of the visual system in first-episode

untreated patients with schizophrenia maybe self-limited: Findings from a secondary small sample follow-up study based on a pilot follow-up study. Psychiatry Res 286:112906.
37. Zhuo C, Xiao B, Chen C, Jiang D, Li G, Ma X, *et al.* (2020): Antipsychotic agents deteriorate brain and retinal function in schizophrenia patients with combined auditory and visual hallucinations: A pilot study and secondary follow-up study. Brain Behav 10:e01611.
38. Zhuo C, Xiao B, Chen C, Jiang D, Li G, Ma X, *et al.* (2021): Abberant inverted U-shaped brain pattern and trait-related retinal impairment in schizophrenia patients with combined auditory and visual hallucinations: A pilot study. Brain Imaging Behav 15:738–747.
39. Zhuo C, Xiao B, Ji F, Lin X, Jiang D, Tian H, *et al.* (2021): Patients with first-episode untreated schizophrenia who experience concomitant visual disturbances and auditory hallucinations exhibit co-impairment of the brain and retinas-a pilot study. Brain Imaging Behav 15:1533–1541.
40. Hilker R, Helenius D, Fagerlund B, Skytthe A, Christensen K, Werge TM, *et al.* (2018): Heritability of schizophrenia and schizophrenia spectrum based on the nationwide Danish twin register. Biol Psychiatry 83:492–498.
41. Trubetskoy V, Pardiñas AF, Qi T, Panagiotaropoulou G, Awasthi S, Bigdeli TB, *et al.* (2022): Mapping genomic loci implicates genes and synaptic biology in schizophrenia. Nature 604:502–508.
42. Gao XR, Huang H, Kim H (2019): Genome-wide association analyses identify 139 loci associated with macular thickness in the UK Biobank cohort. Hum Mol Genet 28:1162–1172.
43. Zhao B, Li Y, Fan Z, Wu Z, Shu J, Yang X, *et al.* (2024): Eye-brain connections revealed by multimodal retinal and brain imaging genetics. Nat Commun 15:6064.
44. Krčmář L, Jäger I, Boudriot E, Hanken K, Gabriel V, Melcher J, *et al.* (2023): The multimodal Munich Clinical Deep Phenotyping study to bridge the translational gap in severe mental illness treatment research. Front Psychiatry 14:1179811.
45. Kalman JL, Burkhardt G, Adorjan K, Barton BB, De Jonge S, Eser-Valeri D, *et al.* (2022): Biobanking in everyday clinical practice in psychiatry-The Munich Mental Health biobank. Front Psychiatry 13: 934640.
46. Sheehan DV, Lecrubier Y, Sheehan KH, Amorim P, Janavs J, Weiller E, *et al.* (1998): The Mini-International Neuropsychiatric Interview (M.I.N.I.): The development and validation of a structured diagnostic psychiatric interview for DSM-IV and ICD-10. J Clin Psychiatry 59(suppl 20):22–33;quiz 34–57.
47. Kay SR, Fiszbein A, Opler LA (1987): The Positive and Negative Syndrome Scale (PANSS) for schizophrenia. Schizophr Bull 13:261–276.
48. Keefe RSE, Goldberg TE, Harvey PD, Gold JM, Poe MP, Coughenour L (2004): The Brief Assessment of Cognition in Schizophrenia: Reliability, sensitivity, and comparison with a standard neurocognitive battery. Schizophr Res 68:283–297.
49. Leucht S, Samara M, Heres S, Davis JM (2016): Dose equivalents for antipsychotic drugs: The DDD method. Schizophr Bull 42(suppl 1):S90–S94.
50. Li K, Wu X, Chen DZ, Sonka M (2006): Optimal surface segmentation in volumetric images-A graph-theoretic approach. IEEE Trans Pattern Anal Mach Intell 28:119–134.
51. Garvin MK, Abràmoff MD, Wu X, Russell SR, Burns TL, Sonka M (2009): Automated 3-D intraretinal layer segmentation of macular spectral-domain optical coherence tomography images. IEEE Trans Med Imaging 28:1436–1447.
52. Abràmoff MD, Garvin MK, Sonka M (2010): Retinal imaging and image analysis. IEEE Rev Biomed Eng 3:169–208.
53. Terry L, Cassels N, Lu K, Acton JH, Margrain TH, North RV, *et al.* (2016): Automated retinal layer segmentation using spectral domain optical coherence tomography: Evaluation of inter-session repeatability and agreement between devices. PLOS ONE 11:e0162001.
54. Robson AG, Frishman LJ, Grigg J, Hamilton R, Jeffrey BG, Kondo M, *et al.* (2022): ISCEV Standard for full-field clinical electroretinography (2022 update). Doc Ophthalmol 144:165–177.
55. Karali T, Padberg F, Kirsch V, Stoecklein S, Falkai P, Keeser D (2021): NAMNIs: Neuromodulation and Multimodal neuroimaging software (0.3). Zenodo. Available at: https://zenodo.org/records/4547552. Accessed December 3, 2022.
56. Eickhoff SB, Paus T, Caspers S, Grosbras MH, Evans AC, Zilles K, Amunts K (2007): Assignment of functional activations to probabilistic cytoarchitectonic areas revisited. Neuroimage 36:511–521.
57. Fischl B, Salat DH, Busa E, Albert M, Dieterich M, Haselgrove C, *et al.* (2002): Whole brain segmentation: Automated labeling of neuroanatomical structures in the human brain. Neuron 33:341–355.
58. Ge T, Chen CY, Ni Y, Feng YA, Smoller JW (2019): Polygenic prediction via Bayesian regression and continuous shrinkage priors. Nat Commun 10:1776.
59. Wold H (1982): Soft modelling: The basic design and some extensions. In: Jöreskog KG, Wold HOA, editors. Systems Under Indirect Observation: Part II. Amsterdam: North Holland Publishing Company, 1–54.
60. Popovic D, Ruef A, Dwyer DB, Antonucci LA, Eder J, Sanfelici R, *et al.* (2020): Traces of trauma: A multivariate pattern analysis of childhood trauma, brain structure, and clinical phenotypes. Biol Psychiatry 88:829–842.
61. Monteiro JM, Rao A, Shawe-Taylor J, Mourão-Miranda J, Alzheimer's Disease Initiative (2016): A multiple hold-out framework for Sparse Partial Least Squares. J Neurosci Methods 271:182–194.
62. McIntosh AR, Lobaugh NJ (2004): Partial least squares analysis of neuroimaging data: Applications and advances. NeuroImage 23(suppl 1):S250–S263.
63. Krishnan A, Williams LJ, McIntosh AR, Abdi H (2011): Partial Least Squares (PLS) methods for neuroimaging: A tutorial and review. NeuroImage 56:455–475.
64. Liang K-Y, Zeger SL (1986): Longitudinal data analysis using generalized linear models. Biometrika 73:13–22.
65. Ying GS, Maguire MG, Glynn R, Rosner B (2017): Tutorial on biostatistics: Linear regression analysis of continuous correlated eye data. Ophthalmic Epidemiol 24:130–140.
66. Pasmanter N, Petersen-Jones SM (2020): A review of electroretinography waveforms and models and their application in the dog. Vet Ophthalmol 23:418–435.
67. Gottesman II, Gould TD (2003): The endophenotype concept in psychiatry: Etymology and strategic intentions. Am J Psychiatry 160:636–645.
68. Gregg RG, Singer J, Kamermans M, McCall MA, Massey SC (2022): Function and anatomy of the mammalian retina. In: Sadda S, Schachat A, Wilkinson C, Hinton D, Wiedemann P, Freund KB, *et al.*, editors. Ryan's Retina, 7th ed. Amsterdam: Elsevier, 378–420.
69. Banitt MR, Ventura LM, Feuer WJ, Savatovsky E, Luna G, Shif O, *et al.* (2013): Progressive loss of retinal ganglion cell function precedes structural loss by several years in glaucoma suspects. Invest Ophthalmol Vis Sci 54:2346–2352.
70. Machida S (2012): Clinical applications of the photopic negative response to optic nerve and retinal diseases. J Ophthalmol 2012: 397178.
71. Marmoy OR, Viswanathan S (2021): Clinical electrophysiology of the optic nerve and retinal ganglion cells. Eye (Lond) 35:2386–2405.
72. Prencipe M, Perossini T, Brancoli G, Perossini M (2020): The photopic negative response (PhNR): Measurement approaches and utility in glaucoma. Int Ophthalmol 40:3565–3576.
73. Adámek P, Langová V, Horáček J (2022): Early-stage visual perception impairment in schizophrenia, bottom-up and back again. Schizophrenia (Heidelb) 8:27.
74. Bernardo M, Cañas F, Banegas JR, Casademont J, Riesgo Y, Varela C, RICAVA Study Group (2009): Prevalence and awareness of cardiovascular risk factors in patients with schizophrenia: A cross-sectional study in a low cardiovascular disease risk geographical area. Eur Psychiatry 24:431–441.
75. Correll CU, Robinson DG, Schooler NR, Brunette MF, Mueser KT, Rosenheck RA, *et al.* (2014): Cardiometabolic risk in patients with first-episode schizophrenia spectrum disorders: Baseline results from the RAISE-ETP study. JAMA Psychiatry 71:1350–1363.

76. de Leon J, Diaz FJ (2005): A meta-analysis of worldwide studies demonstrates an association between schizophrenia and tobacco smoking behaviors. Schizophr Res 76:135–157.
77. McDaid TM, Smyth S (2015): Metabolic abnormalities among people diagnosed with schizophrenia: A literature review and implications for mental health nurses. J Psychiatr Ment Health Nurs 22:157–170.
78. Correll CU, Solmi M, Veronese N, Bortolato B, Rosson S, Santonastaso P, *et al.* (2017): Prevalence, incidence and mortality from cardiovascular disease in patients with pooled and specific severe mental illness: A large-scale meta-analysis of 3,211,768 patients and 113,383,368 controls. World Psychiatry 16:163–180.
79. De Clerck EEB, Schouten JSAG, Berendschot TTJM, Goezinne F, Dagnelie PC, Schaper NC, *et al.* (2018): Macular thinning in prediabetes or type 2 diabetes without diabetic retinopathy: The Maastricht Study. Acta Ophthalmol 96:174–182.
80. Patel PJ, Foster PJ, Grossi CM, Keane PA, Ko F, Lotery A, *et al.* (2016): Spectral-domain optical coherence tomography imaging in 67 321 adults: Associations with macular thickness in the UK Biobank study. Ophthalmology 123:829–840.
81. Khawaja AP, Chua S, Hysi PG, Georgoulas S, Currant H, Fitzgerald TW, *et al.* (2020): Comparison of associations with different macular inner retinal thickness parameters in a large cohort: The UK Biobank. Ophthalmology 127:62–71.
82. Kurtulmus A, Elbay A, Parlakkaya FB, Kilicarslan T, Ozdemir MH, Kirpinar I (2020): An investigation of retinal layer thicknesses in unaffected first-degree relatives of schizophrenia patients. Schizophr Res 218:255–261.
83. Peredo R, Gagné AM, Gilbert E, Hébert M, Maziade M, Mérette C (2020): Electroretinography may reveal cognitive impairment among a cohort of subjects at risk of a major psychiatric disorder. Psychiatry Res 291:113227.
84. Moreau I, Hébert M, Maziade M, Painchaud A, Mérette C (2022): The electroretinogram as a potential biomarker of psychosis in children at familial risk. Schizophrenia Bulletin Open 3:sgac016.
85. Gagné AM, Moreau I, St-Amour I, Marquet P, Maziade M (2020): Retinal function anomalies in young offspring at genetic risk of schizophrenia and mood disorder: The meaning for the illness pathophysiology. Schizophr Res 219:19–24.
86. Maziade M, Bureau A, Jomphe V, Gagné AM (2022): Retinal function and preclinical risk traits in children and adolescents at genetic risk of schizophrenia and bipolar disorder. Prog Neuropsychopharmacol Biol Psychiatry 112:110432.
87. Wahbeh MH, Avramopoulos D (2021): Gene-environment interactions in schizophrenia: A literature review. Genes (Basel) 12:1850.
88. Hanson DR, Gottesman II (2005): Theories of schizophrenia: A genetic-inflammatory-vascular synthesis. BMC Med Genet 6:7.
89. Holopigian K, Clewner L, Seiple W, Kupersmith MJ (1994): The effects of dopamine blockade on the human flash electroretinogram. Doc Ophthalmol 86:1–10.
90. Bartel P, Blom M, Robinson E, Van Der Meyden C, Sommers DK, Becker P (1990): The effects of levodopa and haloperidol on flash and pattern ERGs and VEPs in normal humans. Doc Ophthalmol 76:55–64.
91. Bartel P, Blom M, Robinson E, Van der Meyden C, Sommers DO, Becker P (1990): Effects of chlorpromazine on pattern and flash ERGs and VEPs compared to oxazepam and to placebo in normal subjects. Electroencephalogr Clin Neurophysiol 77:330–339.
92. Filip V, Balík J (1978): Possible indication of dopaminergic blockade in man by electroretinography. Int Pharmacopsychiatry 13:151–156.
93. Perossini M, Fornaro P (1990): Electroretinographic effects induced in humans by psychopharmacologic agents. Doc Ophthalmol 75:1–6.
94. Fornaro P, Perossini M, Placidi GF, Dell'Osso L, Tassi GF, Castrogiovanni P (1984): Electroretinography (ERG) as a tool of investigation on dopaminergic activity in man. Res Commun Psychol Psychiatry Behav 9:307–323.
95. You JY, Dorfman AL, Gauvin M, Vatcher D, Polomeno RC, Little JM, Lachapelle P (2023): Comparing the RETeval® portable ERG device with more traditional tabletop ERG systems in normal subjects and selected retinopathies. Doc Ophthalmol 146:137–150.